JOURNAL OF COMPUTATIONAL PHYSICS 52, 374–389 (1983)

# Shock Simulation by the Particle Method SPH

J. J. MONAGHAN

*Mathematics Department,*
*Monash University, Clayton, Victoria, 3168, Australia*

AND

R. A. GINGOLD

*Mt. Stromlo and Siding Spring Obs.*
*Woden, Private Bag, A.C.T., Australia*

Received September 2, 1982; revised March 15, 1983

The particle method SPH is applied to one-dimensional shock tube problems by incorporating an artificial viscosity into the equations of motion. When the artificial viscosity is either a bulk viscosity or the Von Neumann–Richtmyer viscosity, in a form analogous to that for finite differences, the results show either excessive oscillation or excessive smearing of the shock front. The reason for the excessive particle oscillation is that, in the standard form, the artificial viscosity cannot dampen irregular motion on the scale of the particle separation since that scale is usually less than the resolution of the interpolating kernel. We propose a new form of artificial viscosity which eliminates this problem. The resulting shock simulation has negligible oscillation and satisfactorily sharp discontinuities. Results with a gaussian interpolating kernel (with second-order errors) are shown to be greatly inferior to those with a super gaussian kernel (with fourth-order errors).

## 1. INTRODUCTION

When applying particle methods to the simulation of shocks it is convenient to use the artificial viscosities proposed and tested for finite difference methods (Roache, 1975). These artificial viscosities can be considered as forms of viscous pressure, and they can be easily included in the equations of motion.

In order to calculate the viscous pressure it is first necessary to calculate the divergence of the velocity, $\nabla \cdot \mathbf{v}$. For particle methods which use a grid, $\nabla \cdot \mathbf{v}$ can be calculated by finite differences. For a particle method such as SPH (smoothed particle hydrodynamics) (Gingold and Monaghan, 1977, 1982; Monaghan, 1982) $\nabla \cdot \mathbf{v}$ can be calculated using an interpolating kernel with the particles as interpolating points. The length scales $\nabla \cdot \mathbf{v}$ are therefore bounded below either by the resolution of the grid or the resolution of the interpolating kernel. However, in order to maintain reasonable accuracy, the resolution length scale must be much greater than the typical separation of the particles, and irregular motion on this latter scale is



0021-9991/83 $3.00

then only weakly affected by the artificial viscosity. The scale separation creates problems in shock transitions for two reasons. The first is that in the high-density side of the shock the scale separation is exacerbated. The second is that, in the shock transition, the particles mimic molecules and, in the absence of an appropriate artificial viscosity, the shock is simulated by inducing irregular particle motions on length scales corresponding to the particle separation. Artificial viscosities calculated in the usual way are very inefficient at damping this irregular motion. They can be made to do so by increasing the artificial viscosity, but the result is excessive broadening of the shock front. Experiments confirming these ideas are described in Section 3 of this paper.

It is clear that a particle method requires a damping term which acts more directly on the relative motion of particles. In Section 4 we describe a new artificial viscosity which is equivalent to a bulk viscosity but which acts effectively on irregular motion on the short scale. Experiments described in Section 5 confirm that this artificial viscosity produces negligible oscillation and good resolution of the shock front and contact discontinuity.

Recent theory and experiment with finite difference methods (Van Leer, 1979) show that methods which have third-order accuracy, when used correctly, give excellent results for shock transitions. In this paper we compare results using a gaussian kernel, which has first-order accuracy, with those using a super gaussian kernel which interpolates with third-order accuracy. The latter gives excellent results which rival those found by Sod (1978) for the best of a variety of finite difference methods.

In the following section we establish the equations of motion from the exact equations using the ideas and formalism of Monaghan (1982).

## 2. Equations of Motion

The SPH equations, like those for other particle methods, were first derived by intuitive methods (Lucy, 1977; Gingold and Monaghan, 1977). Recently (Monaghan, 1982) it has been shown how the SPH equations can be derived from the exact equations of motion. The formalism used for this purpose can also be applied to spectral and finite difference methods which are then seen to differ from particle methods by (a) using a different interpolating kernel, and (b) not using (in general) interpolating points which move with the fluid. The main points of the analysis are the following:

(i) All interpolation methods involving linear operations on the function interpolated (e.g., spectral or local polynomial interpolation) can be written in the form

$$\langle A(\mathbf{r})\rangle = \int_D A(\mathbf{r}')\, W(\mathbf{r}, \mathbf{r}', h)\, d\mathbf{r}', \tag{2.1}$$

where $A(\mathbf{r})$ is the function interpolated, $D$ is the domain, and $W$ is a kernel with the following properties:

(a) $$\int_D W(\mathbf{r}, \mathbf{r}', h)\, d\mathbf{r}' \to 1 \qquad \text{as} \quad h \to 0. \tag{2.2}$$

(b) If $A(\mathbf{r})$ is a continuous function

$$\langle A(\mathbf{r}) \rangle \to A(\mathbf{r}) \qquad \text{as} \quad h \to 0. \tag{2.3}$$

The kernel therefore mimics a delta function and it does so more closely as $h \to 0$.

(ii) If the interpolation points are distributed in space with number density $n(\mathbf{r})$ then $\langle A \rangle$ can be approximated by

$$\sum_j \frac{A_j}{n_j} W(\mathbf{r}, \mathbf{r}_j, h), \tag{2.4}$$

where, for any function $B$, $B_j \equiv B(\mathbf{r}_j)$. If the domain is one dimensional, and the points are equi-separated, the choice of an appropriate kernel allows all the standard interpolation formula to be recovered from (2.4). The expression (2.4) for $\langle A \rangle$ is the general SPH interpolation formula.

(iii) Equations for numerical work can be constructed by multiplying each term of the exact equations by the kernel and integrating over the domain where a solution is required. Integration by parts with, if necessary, approximations for nonlinear terms gives the equations for numerical work.

*The Momentum Equation*

We first consider inviscid flow for which the momentum equation is

$$\frac{d\mathbf{v}}{dt} = -\frac{1}{\rho} \nabla p. \tag{2.5}$$

Following (iii) we find

$$\int_D \frac{dv}{dt} W(\mathbf{r}, \mathbf{r}', h)\, d\mathbf{r}' = -\int_D \frac{1}{\rho} \nabla p W(\mathbf{r}, \mathbf{r}', h)\, d\mathbf{r}'. \tag{2.6}$$

It is sufficiently general for most purposes to assume that

$$W(\mathbf{r}, \mathbf{r}', h) \equiv W(|\mathbf{r} - \mathbf{r}'|, h). \tag{2.7}$$

A consequence of this assumption is that for any function $\phi$

$$\langle \nabla \phi \rangle = \nabla \langle \phi \rangle + \int_S \phi(\mathbf{r}')\, W(|\mathbf{r} - \mathbf{r}'|, h)\, \mathbf{n}\, da, \tag{2.8}$$

where the surface integral is over the surface $S$ of the domain $D$. For the problems we consider all the variables vanish on the surface and we can take

$$\langle \nabla \phi \rangle = \nabla \langle \phi \rangle. \tag{2.9}$$

In general, however, surface terms appear in the equations of motion.

Since the RHS of (2.6) involves the nonlinear combination $\nabla p/\rho$ we need further approximations to evaluate the integral. An obvious approximation is to choose

$$\left\langle \frac{d\mathbf{v}}{dt} \right\rangle = -\frac{1}{\langle \rho \rangle} \nabla \langle p \rangle, \tag{2.10}$$

but if exact conservation of linear and angular momentum is required it is better to note that

$$\frac{\nabla p}{\rho} = \nabla \left( \frac{p}{\rho} \right) + \frac{p}{\rho^2} \nabla \rho, \tag{2.11}$$

so that (2.6) can be approximated by

$$\left\langle \frac{d\mathbf{v}}{dt} \right\rangle = -\nabla \left\langle \frac{p}{\rho} \right\rangle - \frac{\langle p \rangle}{\langle \rho \rangle^2} \nabla \langle \rho \rangle. \tag{2.12}$$

No special interpolation method has yet been specified. We now specialize to particle methods. We assign a mass $m$ to each interpolation point and call it a particle, and we move the particle with the acceleration an element of fluid would experience at the position of the particle.

If we assign a mass to each particle the density $\rho$ is given by

$$mn(\mathbf{r}). \tag{2.13}$$

Referring to (2.4) we find (dropping angle brackets for convenience) that (2.12) becomes, at particle $i$,

$$\frac{d\mathbf{v}_i}{dt} = -m \sum_{j=1}^{N} \left( \frac{p_j}{\rho_j^2} + \frac{p_i}{\rho_i^2} \right) \nabla_i W_{ij}, \tag{2.14}$$

where $W_{ij} \equiv W(|\mathbf{r}_i - \mathbf{r}_j|, h)$ and $\nabla_i$ denotes the gradient taken with respect to the coordinate $\mathbf{r}_i$.

An artificial viscosity in the form of a viscous pressure $q$ can be included in the equation of motion by replacing $p$ in (2.14) by $p + q$. The new system of equations conserves total linear and angular momentum exactly.

It can be shown (Monaghan, 1982) that if the same procedure is applied to the

continuity equation it leads to an equation for the time change of the interpolated density

$$\langle \rho(\mathbf{r}) \rangle = m \sum_{j=1}^{N} W(|\mathbf{r} - \mathbf{r}_j|, h) \tag{2.15}$$

which is satisfied automatically locally (that is, at each particle). Total mass is, of course, conserved exactly.

*The Energy Equation*

The energy equation for particle methods can be derived directly from the exact energy equation using the procedure described earlier (Monaghan, 1982). However, in Section 4 we shall introduce an artificial viscosity which is not easily related to a viscous term in the exact equations. It is therefore preferable to construct an energy equation directly from (2.14) and use our knowledge of the exact energy equation to guide the identification of the terms in the energy equation. From (2.14) we find

$$m \sum_i \mathbf{v}_i \cdot \frac{d\mathbf{v}_i}{dt} = -m^2 \sum_i \sum_j \sigma_{ij} \mathbf{v}_i \cdot \nabla_i W_{ij}, \tag{2.16}$$

where

$$\sigma_{ij} := \frac{p_i + q_i}{\rho_i^2} + \frac{p_j + q_j}{\rho_j^2}. \tag{2.17}$$

Interchanging the labels in the double summation we can write (2.16) in the form

$$\sum_i m\mathbf{v}_i \cdot \frac{d\mathbf{v}_i}{dt} = -\frac{m^2}{2} \left\{ \sum_i \sum_j \sigma_{ij} \mathbf{v}_i \cdot \nabla_i W_{ij} + \sum_i \sum_j \sigma_{ji} \mathbf{v}_j \cdot \nabla_j W_{ji} \right\}. \tag{2.18}$$

With the assumptions we have made, $W_{ij} = W_{ji}$, $\sigma_{ij} = \sigma_{ji}$ and $\nabla_i W_{ij} = -\nabla_j W_{ji}$. Accordingly (2.18) can be written in the form

$$\sum_i m\mathbf{v}_i \cdot \frac{d\mathbf{v}_i}{dt} = -\frac{m^2}{2} \sum_i \sum_j \sigma_{ij} \mathbf{v}_{ij} \cdot \nabla_i W_{ij}, \tag{2.19}$$

where $\mathbf{v}_{ij} = \mathbf{v}_i - \mathbf{v}_j$. The LHS of (2.19) is the rate of change of the total kinetic energy. We provisionally identify

$$\frac{m}{2} \sum_j \sigma_{ij} \mathbf{v}_{ij} \cdot \nabla_i W_{ij} \tag{2.20}$$

as the rate of change of thermal energy per unit mass at the position of particle $i$. If our choice is correct (2.20) should be the particle representation of

$$-\frac{p}{\rho} \nabla \cdot \mathbf{v},$$

when $q = 0$. The correspondence can be established by noting that

$$-\frac{p}{\rho}\nabla \cdot \mathbf{v} = -\frac{1}{2}\left[\frac{p}{\rho^2}\{\nabla \cdot (\rho \mathbf{v}) - \mathbf{v} \cdot \nabla \rho\} + \nabla \cdot \left(\frac{\mathbf{v}p}{\rho}\right) - \mathbf{v} \cdot \nabla\left(\frac{p}{\rho}\right)\right]. \quad (2.21)$$

This somewhat surprising combination of terms is suggested by the relation (2.11) which leads to (2.14). If the RHS is converted into the particle form using approximations equivalent to those used in deriving (2.14) we recover (2.20).

If $u_i$ is the thermal energy per unit mass the thermal energy equation is

$$\frac{du_i}{dt} = \frac{m}{2}\sum_j \left(\frac{p_j}{\rho_j^2} + \frac{p_i}{\rho_i^2}\right)\mathbf{v}_{ij} \cdot \nabla_i W_{ij} + \frac{m}{2}\sum_j \left(\frac{q_j}{\rho_j^2} + \frac{q_i}{\rho_i^2}\right)\mathbf{v}_{ij} \cdot \nabla_i W_{ij}, \quad (2.22)$$

where the second term on the RHS of (2.22) is the viscous dissipation.

We could use the energy equation in this form since it would lead to exact energy conservation. It is, however, preferable for our purposes to replace the first term on the RHS of (2.22) by its exact equivalent so that (2.22) can be rewritten so as to give the rate of change of entropy per unit mass $s$:

$$T\frac{ds}{dt} = \frac{m}{2}\sum_j \left(\frac{q_j}{\rho_j^2} + \frac{q_i}{\rho_i^2}\right)\mathbf{v}_{ij} \cdot \nabla_i W_{ij}. \quad (2.23)$$

The advantage of this form is that a relatively crude algorithm for the integration of (2.23) will give satisfactory results over the bulk of the flow. We have, however, used both (2.22) and (2.23) in our calculations and the change in the results is negligible.

*The Artificial Viscosity*

For the present we consider two viscous pressures. These are (a) the Von Neumann–Richtmyer viscous pressure defined by

$$\begin{aligned} q &= \alpha\rho h^2(\nabla \cdot v)^2, & \nabla \cdot v < 0, \\ &= 0, & \nabla \cdot v > 0, \end{aligned} \quad (2.24)$$

where $\alpha$ is a constant, and (b) a bulk viscosity for which

$$\begin{aligned} q &= -\alpha\rho hc\nabla \cdot v, & \nabla \cdot v < 0, \\ &= 0, & \nabla \cdot v > 0, \end{aligned} \quad (2.25)$$

where $\alpha$ is a constant and $c$ is the speed of sound.

Both viscous pressures require the calculation of $\nabla \cdot \mathbf{v}$. In the particle representation we can use either

$$m\sum_j \frac{\mathbf{v}_j \cdot \nabla_i W_{ij}}{\rho_j}, \quad (2.26)$$

or

$$\frac{m}{\rho_i}\sum_j \mathbf{v}_{ji}\cdot\nabla_i W_{ij}, \tag{2.27}$$

where the latter has been derived from the relation

$$\nabla\cdot\mathbf{v}=\frac{1}{\rho}\left[\nabla\cdot(\rho\mathbf{v})-\mathbf{v}\cdot\nabla\rho\right]. \tag{2.28}$$

The expression (2.27) is more accurate than (2.26); in particular it gives the correct result when $\mathbf{v}$ is constant. In the calculations to be described in Section 3 we use (2.27), but the results are very similar to those found when (2.26) is used.

As we noted in Section 1 the estimates of $\nabla\cdot\mathbf{v}$ are only weakly affected by irregular variations of $\mathbf{v}$ on a scale $\ll h$ since the other terms in the summations in (2.26) or (2.27) vary slowly on a scale $\ll h$ and only the average of the irregular variations in $\mathbf{v}$ contributes to $\nabla\cdot\mathbf{v}$. This average is small.

## 3. Numerical Results — Standard Artificial Viscosity

We consider a shock tube problem for a perfect gas analogous to that considered by Sod (1978). The initial conditions are

$$\begin{aligned} &x<0; \quad \rho=1, \quad && p=1\\ &x>0; \quad \rho=0.25, \quad && p=0.2154. \end{aligned} \tag{3.1}$$

In the absence of dissipation the energy equation becomes

$$p=A(s)\rho^{\gamma}, \tag{3.2}$$

with $\gamma=1.4$, and $A(s)=1$ for those particles with $x<0$ initially, and $A(s)=1.25$ for those particles with $x>0$ initially.

For the particle simulation we distribute $N'$ particles uniformly in 0 to 0.6 and $4N'$ uniformly in $-0.6$ to 0.0. Typically we take $N'=80$ and $h$ twice the particle separation in the low-density region. No special boundary conditions are applied at the end points since, for the time elapse we consider, effects at the end points do not have time to propagate to the shock front and contact discontinuity which are near $x=0$.

The time step $\delta t$ is limited by the Courant condition. For the calculations to be discussed here $\delta t=\mathrm{Min}(0.3h/c_i)$, where $c_i$ is the speed of sound ar particle $i$.

The momentum equation was integrated using the leapfrog algorithm. The thermal energy equation (2.23) was integrated by writing it in the form

$$\frac{dA}{dt}=\frac{AQ(\gamma-1)\rho}{p}, \tag{3.3}$$

where $Q$ is the RHS of (2.23), and then updating $A$ with the algorithm

$$A^{(n+1)} = A^{(n)}(1 + \delta t(\gamma - 1)\rho^{(n)}Q/P^{(n)}). \tag{3.4}$$

This algorithm is only first-order accurate in the time but, as shown by the results in Section 5, it gives satisfactory accuracy once the correct artificial viscosity is used. The interpolated pressure is calculated from (3.2) by first calculating $\langle \rho A \rangle$ then setting

$$\langle p \rangle = \langle A\rho \rangle \langle \rho \rangle^{\gamma - 1}. \tag{3.5}$$

For these calculations we use two interpolating kernels. The first is the gaussian

$$W(u, h) = \frac{1}{h\sqrt{\pi}} e^{-u^2/h^2}, \tag{3.6}$$

which gives an interpolation error of $O(h^2)$. The second is the super gaussian

$$W(u, h) = \frac{1}{h\sqrt{\pi}} e^{-u^2/h^2} \left(\frac{3}{2} - u^2/h^2\right), \tag{3.7}$$

which gives interpolation errors of $O(h^4)$. For a given $h$ the super gaussian kernel has a better resolution than the gaussian kernel (3.6). When the kernel, or its derivative, is required in the computation it is obtained by interpolation from an array. For this reason the CPU time is independent of the kernel.

The expressions for the density, acceleration and viscous dissipation formally involve a summation over all the particles. In practice this summation need only include particles out to $3h$. A substantial saving in time is achieved when $N'$ is large ($\gtrsim 150$) by using cells as a bookkeeping device. If the particles are assigned to cells of width $3h$, and identified through linked lists, the calculation time is proportional to $N$ and not $N^2$ as it would be if the complete summation was performed. The procedure for carrying this out is described in detail by Hockney and Eastwood (1981) in their discussion of short-range forces in particle simulation models. The resulting algorithm is nearly as quick as PIC, but has the advantage that the spatial resolution is superior since it is approximately the particle separation not the cell width as in PIC.

The results for a typical calculation with the Von Neumann–Richtmyer and bulk viscosities are compared with the exact solution in Fig. 1. The calculations use the super gaussian kernel (3.7) with $h = 0.015$. The numerical results show good agreement with the exact solution for $p$ and $\rho$, but the shock front is broadened over $\sim 4h$. The velocity shows the irregular oscillations discussed earlier. These oscillations, being irregular and of short wavelength, have little effect on the $p$ and $\rho$ profiles. The oscillations are particularly large in the case of the bulk viscosity (2.25) where the amplitude of the oscillation reaches 30 percent of the correct velocity. By increasing $\alpha$ by a factor 4 the post shock oscillations are reduced to $\sim 10$ percent, but

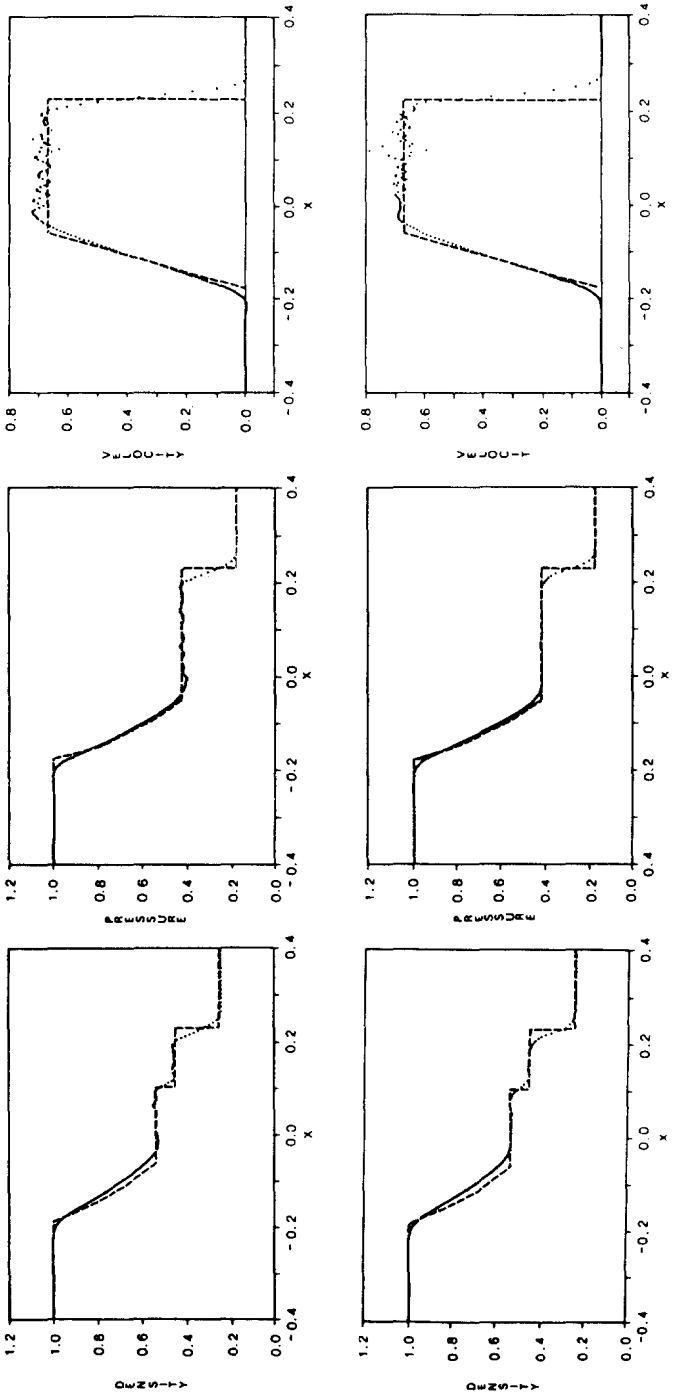


FIG. 1. Pressure, density, and velocity profiles for the shock tube problem described in Section 3 with $N = 80$ and $h = 0.015$. The upper frames are for the Von Neumann–Richtmyer viscosity. The lower frames are for the bulk viscosity. The exact results are shown: ——. The SPH results are shown by dots and full lines. The calculation uses the super gaussian kernel.

the shock is broadened over $10h$. More regular oscillations appear when the Von Neumann–Richtmyer viscosity is used. In this case a large fraction of the energy in the oscillations is associated with a length scale $\gtrsim h$ and, as a consequence, the oscillations show up in the $p$ and $\rho$ profiles. As before the oscillations can be removed by increasing $\alpha$ sufficiently, but the broadening of the shock front becomes unacceptably large.

For a given $\alpha$ the oscillation increase in amplitude as the magnitude of the initial discontinuity is increased. In the next section we discuss the construction of an alternative artificial viscosity which removes the oscillation while retaining good resolution of the discontinuities.

## 4. The New Artificial Viscosity

The results described in Section 3 show the need for an artificial viscosity which acts more directly on the relative motion of the particles. The following intuitive arguments are those that led us to an appropriate form of artificial viscosity.

We need to replace the factor

$$\frac{p_i}{\rho_i^2}+\frac{p_j}{\rho_j^2}$$

by

$$\frac{p_i}{\rho_i^2}+\frac{p_j}{\rho_j^2}+\Pi_{ij}, \tag{4.1}$$

where $\Pi_{ij}$ is the new term which acts as an artificial viscosity. To keep the analysis simple we confine our attention to motion in one dimension and look for a $\Pi_{ij}$ that is similar to a bulk viscosity. We expect $\Pi_{ij}$ to be an approximation to

$$-\alpha\frac{hc}{\rho}\frac{\partial v}{\partial x},$$

which is sensitive to the relative motion of two particles on a scale $<h$. Since

$$\frac{v_{ij}}{x_{ij}}=\frac{v_i-v_j}{x_{ij}}=\frac{1}{x_{ij}}\left[v_i-\left(v_i+x_{ji}\frac{\partial v_i}{\partial x_i}+\cdots\right)\right]\sim\frac{\partial v_i}{\partial x_i}, \tag{4.2}$$

we could try

$$\Pi_{ij}=-\alpha\frac{hc_1}{\rho_i}\frac{v_{ij}}{x_{ij}}. \tag{4.3}$$

However, (4.3) has two deficiencies: (a) the $x_{ij}$ in the denominator might lead to a

viscous force which is too large and (b) $\Pi_{ij} \neq \Pi_{ji}$ so that linear momentum is not automatically conserved. To correct the first deficiency we replace

$$\frac{1}{x_{ij}} \quad \text{by} \quad \frac{x_{ij}}{x_{ij}^2 + \varepsilon h^2}, \tag{4.4}$$

where $0 < \varepsilon \ll 1$, and in practice we find $\varepsilon \lesssim 0.1$ is adequate for the numerical experiments we describe here. When the density contrast is larger a smaller $\varepsilon$ is appropriate. The general rule is that if the initial particle separation on the high-density side is $f$ times that on the low-density side then $\varepsilon \sim f^2$.

To correct the second deficiency we replace $c_i$ and $\rho_i$ by $\bar{c}_{ij}$ *and* $\bar{\rho}_{ij}$, respectively, where, for any function $B$, we define

$$\bar{B}_{ij} := \tfrac{1}{2}(B_i + B_j). \tag{4.5}$$

The final expression for $\Pi_{ij}$ is

$$\begin{aligned} \Pi_{ij} &= -\alpha \frac{h\bar{c}_{ij}}{\bar{\rho}_{ij}} \frac{v_{ij}x_{ij}}{x_{ij}^2 + \varepsilon h^2}, & v_{ij}x_{ij} < 0, \\ &= 0, & v_{ij}x_{ij} > 0, \end{aligned} \tag{4.6}$$

where $v_{ij}x_{ij}$ is used to determine whether $\partial v/\partial x$ is positive or negative. The artificial viscosity is only needed in the latter case. In particle terms the viscosity only operates on approaching particles. If the kernel is the gaussian (3.6) the total viscous acceleration is

$$-\frac{2m\alpha}{h} \sum_j \frac{\bar{c}_{ij}}{\bar{\rho}_{ij}} \frac{v_{ij}x_{ij}^2}{x_{ij}^2 + \varepsilon h^2} W_{ij}. \tag{4.7}$$

We can write (4.7) in a form which is simple to interpret by defining

$$\sigma_{ij} := \frac{\bar{c}_{ij}x_{ij}^2 W_{ij}}{\bar{\rho}_{ij}(x_{ij}^2 + \varepsilon h^2)}, \tag{4.8}$$

and

$$\sigma_i := \sum_j \sigma_{ij}. \tag{4.9}$$

With the use of $\sigma_{ij}$ and $\sigma_i$ we can write (4.7) in the form

$$-\frac{2m\alpha\sigma_i}{h}(v_i - \bar{v}_i), \tag{4.10}$$

where

$$\bar{v}_i = \frac{\sum_j \sigma_{ij} v_j}{\sum_j \sigma_{ij}}. \tag{4.11}$$

Expression (4.10) shows that the viscous force attempts to drive $v_i$ to $\bar{v}_i$, where the latter is an average velocity taken with weight $\sigma_{ij}$. Expression (4.10) bears a formal similarity to the viscosity used by Marder (1975), who, however, uses a different definition of $\bar{v}_i$ and a different rule for specifying the coefficient multiplying $(v_i - \bar{v}_i)$. Furthermore, since Marder uses a grid with approximately 10 particles per cell, the resolution in his calculations is ~5 times coarser than can be achieved by the SPH calculations.

In the appendix we show that if $h$ is sufficiently small, and summations are replaced by integrations, the viscous acceleration is

$$\frac{1}{2}\alpha\frac{h}{\rho}\frac{\partial}{\partial x}\left(\rho c\frac{\partial v}{\partial x}\right),$$

which establishes, as expected, that the artificial viscosity is approximately equivalent to a bulk viscosity in the exact equations.

The energy equation we use is (2.23) with $\Pi_{ij}$ instead of $(q_i/\rho_i^2 + q_j/\rho_j^2)$.

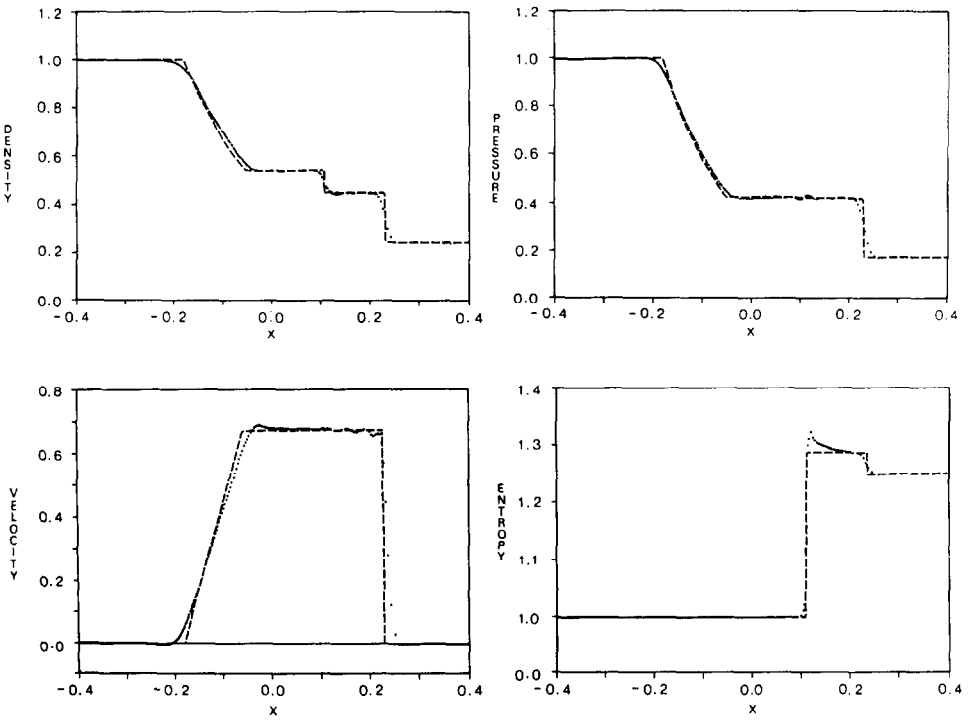


FIG. 2. As for Fig. 1 except that the SPH calculation uses the new artificial viscosity. The kernel is super gaussian.

## 5. Numerical Results — New Viscosity

The numerical results for the shock tube problem described in Section 3 using the SPH method with $\Pi_{ij}$ are illustrated in Fig. 2. For this calculation the super gaussian kernel (3.7) was used. The results are much better than those found using the standard artificial viscosity. The shock front and contact discontinuity are now broadened over only $2h$, which improves on the results discussed in Section 3 and rivals the best of the methods discussed by Sod (1978). By comparison with the results in Section 3 oscillations are negligible. The end points of the rarefaction wave are not perfectly sharp but the error is small.

The pressure profile shows a weak blip at the contact discontinuity. It is due to the fact that the variable $A$ is discontinuous at the contact discontinuity, and when $\langle A\rho \rangle$ is formed it is inevitable that $\langle p \rangle$ is slightly lower to the left of the contact discontinuity, and slightly higher to the right. This blip increases with increase in the jump in $A$ at the contact discontinuity, but it has a negligible effect on the motion.

In recent experiments we have found that if the pressure acceleration term $\nabla p/\rho$ is written in the form

$$\rho^{\gamma-2}\{\nabla(A\rho) + (\gamma - 1)A\nabla\rho\}$$

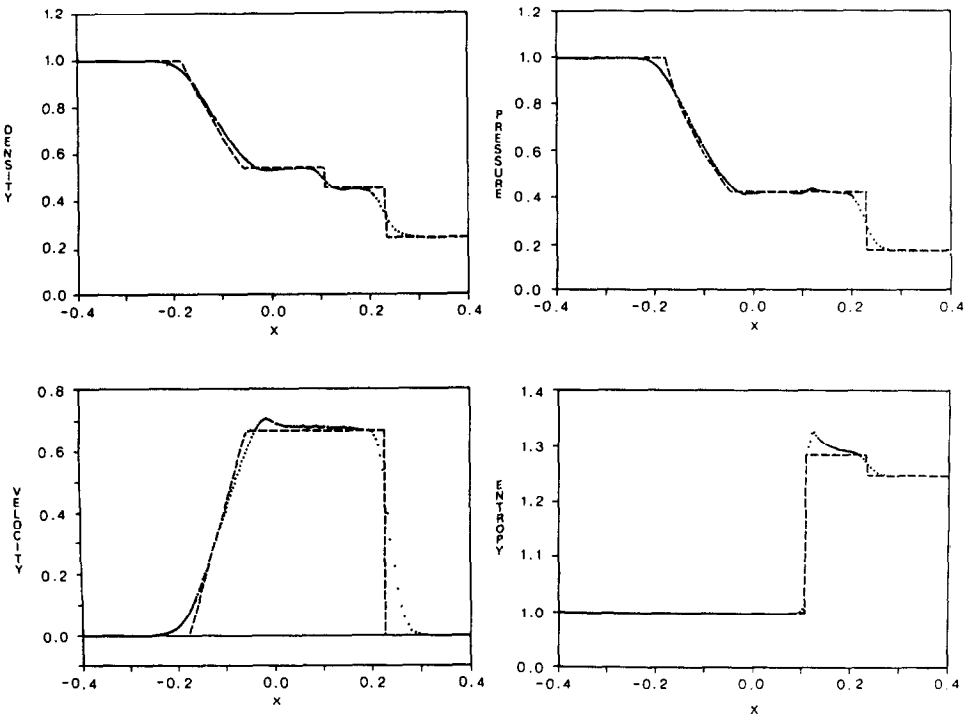


FIG. 3. As for Fig. 2 except that a normal gaussian kernel was used.

the resulting equations of motion give results comparable in accuracy to those described here without the blip in the pressure curve.

In Fig. 3 we show the results for the same problem using the gaussian kernel (3.6). The shock front and contact discontinuity are now broadened over $3h$, and the end points of the rarefaction wave are more rounded. If the same kernel is used with the standard viscosities the results are inferior to those shown in Fig. 3 and they show the excessive oscillation in the velocity already noted in Section 3. These results might be expected because the standard gaussian kernel interpolates with lower accuracy than the super gaussian kernel. However, a priori estimates of accuracy are difficult because in particle methods there are two sources of interpolation error. One of these is the truncation error known to be greater for the standard gaussian kernel. The other source of error is the estimate of integrals by sums, as in passing from (2.1) to (2.4). We are uable to estimate how this latter error is affected by changing the kernel. It is clear, however, that in practice the super gaussian kernel is superior.

## 6. Generalization

The artificial viscosity term can be easily generalized to an arbitrary number of dimensions by writing it in the form

$$\Pi_{ij} = -\frac{\alpha h \bar{c}_{ij}}{\bar{\rho}_{ij}} \frac{\mathbf{v}_{ij} \cdot \mathbf{r}_{ij}}{r_{ij}^2 + \varepsilon h^2}, \qquad \mathbf{v}_{ij} \cdot \mathbf{r}_{ij} \leqslant 0,$$

$$= 0, \qquad \mathbf{v}_{ij} \cdot \mathbf{r}_{ij} > 0.$$

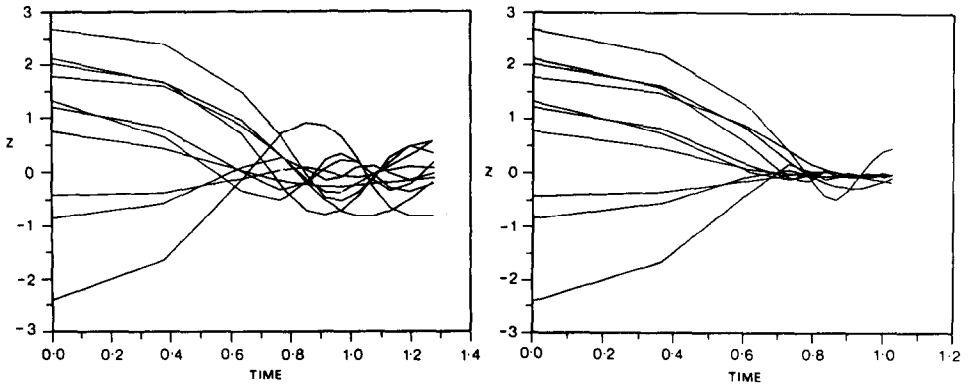


FIG. 4. The variation of the $z$ coordinate with time for some selected particles in the three-dimensional collapse of an isothermal self-gravitating cloud rotating about the $z$ axis. The frame on the left shows the collapse with no artificial viscosity and illustrates vigorous streaming through the equatorial plane. The frame on the right shows the collapse when the new artificial viscosity is used in the $z$ component of the momentum equation. The streaming is now negligible.

In some problems (for example, the collapse of rotating, self-gravitating clouds) where the correct transport of angular momentum is important, it is preferable to include $\Pi_{ij}$ only in the component of the momentum equation which is parallel to the angular momentum vector (Gingold and Monaghan, 1982), and replace $\mathbf{v}_{ij} \cdot \mathbf{r}_{ij}$ by $\mathbf{u}_{ij} \cdot \mathbf{r}_{ij}$, where $\mathbf{u}_i$ is the velocity component of particle $i$ parallel to the angular momentum vector. In that context $\Pi_{ij}$ has the further advantage that it acts very effectively to prevent unwanted particle streaming. As an example we show in Fig. 4 the $z$ coordinates for particles in a collapsing, rotating cloud both with and without the artificial viscosity.

A further extension of the ideas described in Section 4 is to construct a $\Pi_{ij}$ for a viscosity equivalent to the Von Neumann–Richtmyer viscosity. In one dimension the appropriate $\Pi_{ij}$ is

$$\frac{\alpha h^2 v_{ij}^2}{\bar{\rho}_{ij}(x_{ij}^2 + \varepsilon h^2)},$$

where $\alpha$ is a constant.

Experiments with this $\Pi_{ij}$ produce results very similar to those described in Section 5.

## 7. Conclusions

Our numerical experiments show that it is possible to choose an artificial viscosity for the particle method SPH which results in negligible post shock oscillations. If a kernel which interpolates with third-order accuracy is used, the discontinuities are resolved with an overall accuracy that rivals the best of the methods considered by Sod (1978), but it is not quite as accurate as Van Leer's (1979) method. The present method has the advantage that it is very easy to apply, and its generalization and application to more than one dimension are straightforward.

## Appendix

The viscous acceleration in one dimension is

$$a_v = m\alpha h \sum_j \frac{\bar{c}_{ij}}{\bar{\rho}_{ij}} \frac{v_{ij} x_{ij}}{x_{ij}^2 + \varepsilon h^2} \nabla_i W_{ij}, \tag{A.1}$$

where $\nabla_i$ is now equivalent to $\partial/\partial x_i$. Since the presence of $W_{ij}$ limits the contribution to the summation to those points with $x_j \sim x_i$ we expand the variables about this point. Thus

$$v_{ij} = x_{ij} v_i' - \frac{x_{ij}^2}{2} v_i'' + \cdots, \tag{A.2}$$

$$\frac{\bar{c}_{ij}}{\bar{\rho}_{ij}} = \frac{c_i}{\rho_i} + \frac{x_{ji}}{2}\left(\frac{c}{\rho}\right)'_i + \cdots, \tag{A.3}$$

where, for any function $B(x)$, $B'_i \equiv \partial B(x_i)/\partial x_i$. If (A.2) and (A.3) are substituted into (A.1) and the following results are used,

(i) $$m\sum_j \frac{x_{ij}^2 \nabla_i W_{ij}}{x_{ij}^2 + \varepsilon h^2} \doteq \sum_j \nabla_i W_{ij} \doteq \langle \rho \rangle'_i, \tag{A.4}$$

and

(ii) $$\begin{aligned} m\sum_j \frac{x_{ij}^3 \nabla_i W_{ij}}{x_{ij}^2 + \varepsilon h^2} &\doteq m\sum_j x_{ij} \nabla_i W_{ij} \\ &= x_i m \sum_j \nabla_i W_{ij} - \nabla_i \left( m \sum x_j W_{ij} \right) \\ &\doteq x_i \langle \rho \rangle'_i - \langle x\rho \rangle'_i \\ &\doteq \langle \rho \rangle_i . \end{aligned} \tag{A.5}$$

(A.1) becomes (dropping angle brackets for convenience)

$$-\frac{\alpha h}{2\rho_i}\frac{\partial}{\partial x_i}(\rho c v')_i + O(h^p). \tag{A.6}$$

The error depends on how well $\langle A \rangle$ represents $A$ and how well (2.4) approximates (2.1). The first source of error is a truncation error (Monaghan, 1982) which for the kernel (3.6) is of order $h^2$ and for the kernel (3.7) is of order $h^4$.

## References


R. A. Gingold and J. J. Monaghan, *Mon. Not. Roy. Astron. Soc.* **181** (1977), 375–389.

R. A. Gingold and J. J. Monaghan, *J. Comput. Phys.* **46** (1982), 429–453.

R. W. Hockney and J. W. Eastwood, "Computer Simulation Using Particles," McGraw–Hill, New York, 1981.

B. M. Marder, *Math. Comp.* **29** (1975), 434.

J. J. Monaghan, *SIAM. J. Sci. Statist. Comput.* **3** (1982), 422.

P. J. Roache, "Computational Fluid Dynamics," Hermosa Pub., Albuquerque, 1975.

G. A. Sod, *J. Comput. Phys.* **27** (1978), 1–31.

B. Van Leer, *J. Comput. Phys.* **32** (1979), 101–136.